Hydrazine-nitrate combustion synthesis of BaCeO3 preceramic powders: structure, morphology and thermophysical properties

Maksim Tenevich (m.tenevich@mail.ioffe.ru)
Ioffe Institute: FBGUN Fiziko-tehniceskij institut imeni A F Ioffe Rossijskoj akademii nauk
https://orcid.org/0000-0003-2003-0672
Andrey Pavlovich Shevchik
Saint-Petersburg State Institute of Technology: Sankt-Peterburgskij gosudarstvennyj tehnologiceskij institut (tehniceskij universitet)
Vadim Igorevich Popkov
Ioffe Institute: FBGUN Fiziko-tehniceskij institut imeni A F Ioffe Rossijskoj akademii nauk

Research Article

Keywords: solution combustion synthesis, hydrazine, barium cerate, SOFC, thermal diffusivity, thermal conductivity

Posted Date: June 11th, 2021

DOI: https://doi.org/10.21203/rs.3.rs-607249/v1

Version of Record: A version of this preprint was published at Journal of Sol-Gel Science and Technology on January 14th, 2022. See the published version at https://doi.org/10.1007/s10971-021-05717-5.

Hydrazine-nitrate combustion synthesis of $BaCeO_3$ preceramic powders: structure, morphology and thermophysical properties

M.I. Tenevich[1], A.P. Shevchik[2], V.I. Popkov[1]

[1] Ioffe Institute, 194021, Saint Petersburg, Russian Federation

[2] Saint-Petersburg State Institute of Technology, 190013, Saint Petersburg, Russian Federation

Abstract

In the present work, preceramic nanocrystallite barium cerate ($BaCeO_3$) was successfully synthesized using the hydrazine-nitrate combustion method. Using carbon-free hydrazine (N_2H_4) as fuel significantly reduced the formation of carbon by-products. Characterization of the as-received powders was performed by XRD, energy-dispersive X-ray spectroscopy (EDXS), scanning electron microscopy (SEM), simultaneous thermal analysis (DTA-TGA) and adsorption-structural analysis (N_2, 77 K). Thermophysical properties of the sample annealed at 1000 °C were investigated using laser flash analysis (LFA) in the temperature interval of 1000 °C. As a result of a comprehensive study, the sequence of chemical and phase transformations that lead to the formation of $BaCeO_3$ with a rhombic structure (*Pnma*, a = 6.2145 Å, b = 8.7776 Å, c = 6.2337 Å) during the thermal processing of combustion products was investigated. It was established that the average size of the obtained nanocrystals is 38±3 nm and that they form micron-sized agglomerates with a specific surface area of the powder of 4.8 m^2/g. It was shown that the sintered sample of $BaCeO_3$ is characterized by thermal diffusivity values of 0.28 to 0.20 mm^2/s and thermal conductivity values of 0.41 to 0.35 W/mK, depending on temperature. These results, given the impact of porosity on the sample (~ 40%), show very good agreement with the thermophysical characteristics of densely sintered ceramics based on $BaCeO_3$ – a solid oxide electrolyte SOFC. Consequently, the proposed method of hydrazine-nitrate synthesis of $BaCeO_3$ presents itself as a promising approach to obtaining preceramic powders and ceramics in the area of SOFC.

Keywords: solution combustion synthesis, hydrazine, barium cerate, SOFC, thermal diffusivity, thermal conductivity

1. Introduction

A solid oxide fuel cell (SOFC) is a device that allows converting the energy of chemical bonds into electric energy both effectively and ecologically. According to the general classification, there

exist three types of SOFC materials: high-temperature (600-1000 °C), intermediate-temperature (500-750 °C), and low-temperature (≤450 °C) [1]. Among them, high-temperature SOFCs are the most effective and productive, but their use is greatly restricted by problems in the exploitation of materials and devices in such temperatures. Therefore decreasing the working temperature of SOFC to the intermediate-temperature area while maintaining their high level of effectiveness and productivity is a most relevant question. It directly translates into the need to develop new solid oxide materials that would exhibit a range of chemical, thermophysical, proton-conducting, and other properties.

The main components of SOFC are electrodes (cathode and anode) and an electrolyte. The electrolyte material must satisfy several criteria such as high ionic conductivity, low electronic conductivity, chemical and physical stability under reducing and oxidizing atmospheres at the operating temperature and oxidizing atmospheres at operating temperature, and ease of preparation in the form of a dense film. At present, the key electrolyte materials with proton conductivity include YSZ, Co-doped ceria, doped lanthanum silicate apatite, molybdenum oxides (ionic conductivity), BaZr- or/and BaCe-based mixed oxides, lanthanum tungstates [2–4]. Typically, the active components in SOFC are complex oxides with perovskite structures that, owing to their crystalline structures, exhibit high ionic conductivity. Perovskite materials are used in developing every element of SOFC – as cathodes[5], anodes[6,7], and electrolyte materials [2,8].

Among these materials, of particular interest is barium cerate $BaCeO_3$. The complex oxide perovskite $BaCeO_3$ has fascinated researchers for over 30 years [9]. These types of proton conductors can be used as electrolyte material for intermediate-temperature (500–750 °C) solid oxide fuel cells (IT-SOFCs). There are, however, several challenges related to the process of yielding single-phase preceramic and ceramic materials based on barium cerate in those cases when it becomes necessary to dope it with other elements. One of the most basic methods of yielding barium cerate is solid-phase synthesis. The main disadvantages of this method are low homogeneity, the complexity of size control for material particles high sintering temperatures, and long sintering time [10–12]. The second group of technologies is solution-based methods including co-precipitation, combustion methods (fuel–nitrate combustion), sol-gel Pechini methods, cryochemical and hydrothermal syntheses, and others [11,13–19]. The main advantages of these technologies are the considerably smaller size of particles of prepared powders and their high homogeneity, which favors the decrease in synthesis temperature and duration of phase formation of multicomponent compounds, as well as preparation of gastight ceramic products at lower sintering temperatures.

Comparison of data on preceramic barium cerate powders revealed that the size of the crystallites in the case of solid-phase synthesis is 45-47 nm, and by the method of solution

combustion - 240 nm, 97 nm. The specific surface area is 4.46 m^2/g [20], 3.4 m^2/g [21], 3 m^2/g [22] and 3 m^2/g. Density in solid-phase synthesis does not exceed 70% and the sintering process requires a lot of power and time. By co-precipitation of oxalates, a density of 85-90% can be obtained. The solution combustion method that involves the use of various dopants can achieve a density of >95%.

The method of solution combustion allows obtaining nanopowders of simple and complex oxides with the desired crystalline structure and size parameters via both direct synthesis and synthesis involving thermal processing of amorphous combustion products [23–25]. Advantages of this method include simplicity, short duration, and the possibility to inject large amounts of dopants while preserving the single-phaseness of the products of synthesis. This method has been widely studied [26–28] and employed in synthesizing a whole range of complex oxide systems. [29–33]. Components of this method include water solutions of nitrates acting as an oxidizer and organic fuel acting as a reducing agent. The main types of fuel include urea, glycine, citric acid, and others. [9]. One of the disadvantages of this method consists in the presence of carbon residue in combustion products, which results from the incomplete oxidation of carbon-filled fuel. During barium cerate synthesis, this may lead to the formation of various carbonate by-products and require raising the temperature to stabilize the annealing and obtain a single-phase product. For this reason, hydrazine (N_2H_4), known as a constituent in rocket fuels that helps preserve solution combustion, presents itself as a promising carbon-free fuel.

On this basis, it is essential to develop new original methods for obtaining barium cerate particles characterized by nano-size and low specific surface area with a high degree of aggregation.

In this work, we put forth and test the hydrazine-nitrate combustion method of obtaining single-phase preceramic nanopowders based on $BaCeO_3$ via thermal processing of combustion products. We then analyze the range of physicochemical processes that accompany the formation of barium cerate. Finally, we analyze the functional characteristics of the as-obtained products using adsorption-structural analysis, sol-gel Pechini methods, as well as using X-ray dispersion to analyze thermophysical properties. Based on the conclusions of these analyses, we discuss possible implementations of this method in obtaining advanced ceramic SOFC materials.

2. Experimental

2.1 Materials

Barium nitrate $Ba(NO_3)_2$ 99.55% (chemically pure) and nitric acid HNO_3 70% (chemically pure) were purchased from the Neva Reaktiv. Cerium nitrate hexahydrate $Ce(NO_3)_3 \cdot H_2O$ >99%

(chemically pure) was purchased from the ChemCraft. Hydrazine hydrate $N_2H_4 \cdot H_2O$ (Germany) was purchased from Lenreactiv. All chemical reagents were used without further purification.

2.2 Synthesis

Preceramic barium cerate powder was obtained via hydrazine-nitrate combustion with subsequent annealing in air at wide temperature intervals. The sintered pellet of barium cerate was obtained from preceramic powder by pressing and sintering.

2.2.1 Solution combustion synthesis

Analytically pure $Ba(NO_3)_2$, $Ce(NO_3)_3 \cdot 6H_2O$ and $N_2H_4 \cdot H_2O$ were used as initial materials without further purification. An appropriate amount of $Ba(NO_3)_2$ and $Ce(NO_3)_3 \cdot 6H_2O$ (hydrazine to nitrate ratio calculated as 1.2 (stoichiometry)) were separately dissolved in distilled water. Next, the required amount of $N_2H_4 \cdot H_2O$ was added to the barium nitrate solution under magnetic stirring. Nitric acid was added to a mixture of barium nitrate and hydrazine to reach pH=1. After $Ce(NO_3)_3 \cdot 6H_2O$ was added to the mixture $Ba(NO_3)_2$ - $N_2H_4 \cdot H_2O$ - HNO_3.
The reaction equation is shown below Eq. (1):

$$2Ba(NO_3)_2 + 2Ce(NO_3)_3 \cdot 6H_2O + 12N_2H_4 \cdot H_2O = 2BaCeO_3 + 17N_2 + 48H_2O \quad (1)$$

The resulting mixture was stirred and heated on a hotplate at 350 °C until it became a high viscous gel. With further exposure, the gel self-ignited with the formation of a powder.

2.2.2 Thermal treatment of powder and pellet quenching

The obtained powder precursor was annealed in air at 500, 600, ..., 1000 °C for 4 h. Next, the sample annealed at 1000 °C was pressing in a pellet at a pressure of 25 bar and sintered at the final temperature of 1000 °C in an electric furnace in the air by heating to the final temperature at 20 °C/min and holding there for 4 hours.

2.3 Characterization

The morphology of the synthesized compositions and their chemical compositions were investigated by scanning electron microscopy (SEM), energy-dispersive X-ray spectroscopy (EDXS) using a Tescan Vega 3 SBH scanning electron microscope, equipped with an Oxford INCA X-act X-ray spectral microanalysis attachment.

X-ray phase and X-ray structural analyses were conducted using a Rigaku SmartLab 3 Powder X-ray diffractometer, and phase analysis of the compositions was performed using the PDF-2 ICDD. To exclude an instrumental error, the imaging was performed using an internal

standard (SiC powder). Specifying the parameters of a unit cell, X-ray density and size of crystallites was performed with the help of Rigaku SmartLab 3 software and the Rietveld method by Bourevestnik, which allows measuring the parameters of the unit cell of multiphase systems with high accuracy.

Simultaneous thermogravimetric (TG) and differential thermal analysis (DTA) measurements in air atmosphere were achieved in flowing mode with heating rates of 10 °/min up to 1000 °C using a Netzsch STA 449 F3 Jupiter instrument.

2.4 Functional properties

Temperature conductivity α(T) and thermal conductivity λ(T) were measured using the NETZSCH LFA 457 MicroFlash system. Thermodynamic data about temperature dependence of relative thermal capacity of $BaCeO_3$ was taken from work [29].

The specific surface of the sample was determined by the low-temperature nitrogen (N_2) sorption-desorption method. The isotherm was obtained at the temperature of liquid nitrogen (77 K) using a Micromeritics ASAP 2020 analyzer.

The pycnometric density was measured by the helium pycnometry performed using a Micromeritics Ultra Pycnometer 1000, in a 1 cm^3 microcell in a regime with degassing of the specimen in a helium flow with degassing time of 10 min. The bulk density was measured using a Micrometritics GeoPyc 1365.

Porosity measurements were performed by the following formula (Eq. 2-4):

$$P_{open} = \left(1 - \frac{\rho_{pyc}}{\rho_{XRD}}\right) \cdot 100 \qquad (2)$$

$$P_{sum} = (1 - \frac{\rho_{bulk}}{\rho_{XRD}}) \cdot 100 \qquad (3)$$

$$P_{close} = P_{sum} - P_{open} \qquad (4)$$

Where P_{open} stands for open porosity, P_{sum} - general porosity, P_{close} - closed porosity, ρ_{pyc} - pycnometric density, ρ_{XRD} - X-ray density, and ρ_{bulk} - apparent density.

3. Results and discussion

3.1 Formation mechanism of $BaCeO_3$

The results of the elemental analysis of powder calcined at 1000 °C are shown in Fig. 1. According to this data, the composition of the powder contains no impurity elements, and the spectral lines correspond to barium (Ba), cerium (Ce) and oxygen (O). The presence of carbon lines is linked to the specificities of sample preparation (using carbon substrate). Quantitative

analysis of this spectrum indicates that the proportions of key elements are in correspondence with the stoichiometry of barium cerate $BaCeO_3$.

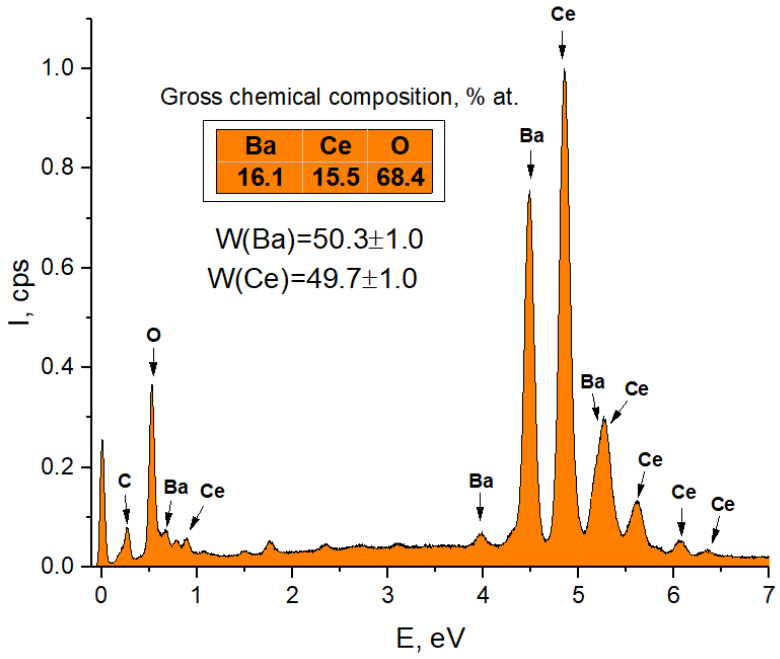

Fig. 1 Energy dispersive spectrum of $BaCeO_3$-based sample annealed at 1000 °C

To investigate the physicochemical processes occurring during the synthesis of preceramic powders of barium cerate from the products of hydrazine-nitrate combustion, a synchronic thermal analysis (DTA-TGA) of the as-prepared sample was conducted. The results are shown in Fig. 2. According to this data, the thermogram shows 3 main regions at the following temperature intervals: R.T. - 300 °C, 500 - 650 °C and 650 - 850 °C.

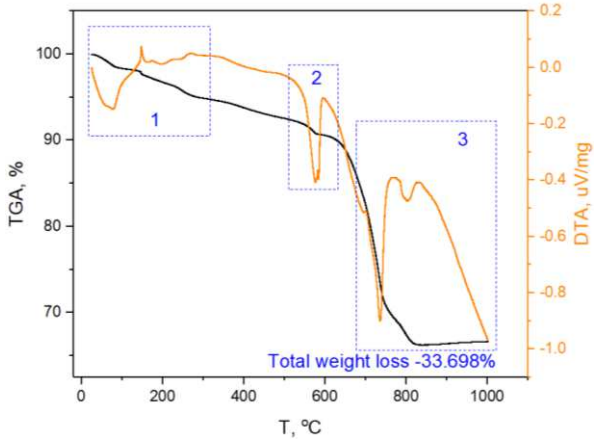

Fig. 2 TGA-DTA thermograms of the as-prepared sample

In the first region of temperatures of up to 300 °C, there occurs the removal of physically and chemically linked water.

In the second temperature range from 500 to 650 ° C, barium nitrate melts. The loss of mass in the first 2 regions was approximately 10%.

In the third region of temperatures, the thermal effect at 650-800 °C was caused by the decomposition of barium nitrate [32]. The endothermic effect in the region of 800-900 °C is associated with the decomposition of barium carbonate.

It is worth noting that the exothermic effect of the formation of $BaCeO_3$ does not appear in the thermogram, which results from its overlapping with the intense endothermic effects of the decomposition of nitrates. No thermal effects or changes in the mass of the sample were observed at temperatures greater than 850 °C.

Obtaining pre-ceramic barium cerate powder in these conditions was confirmed using X-ray diffraction, which allowed to investigate the particularities of phase transformations in the examined system during heat treatment of up to 1000 °C (Fig. 3).

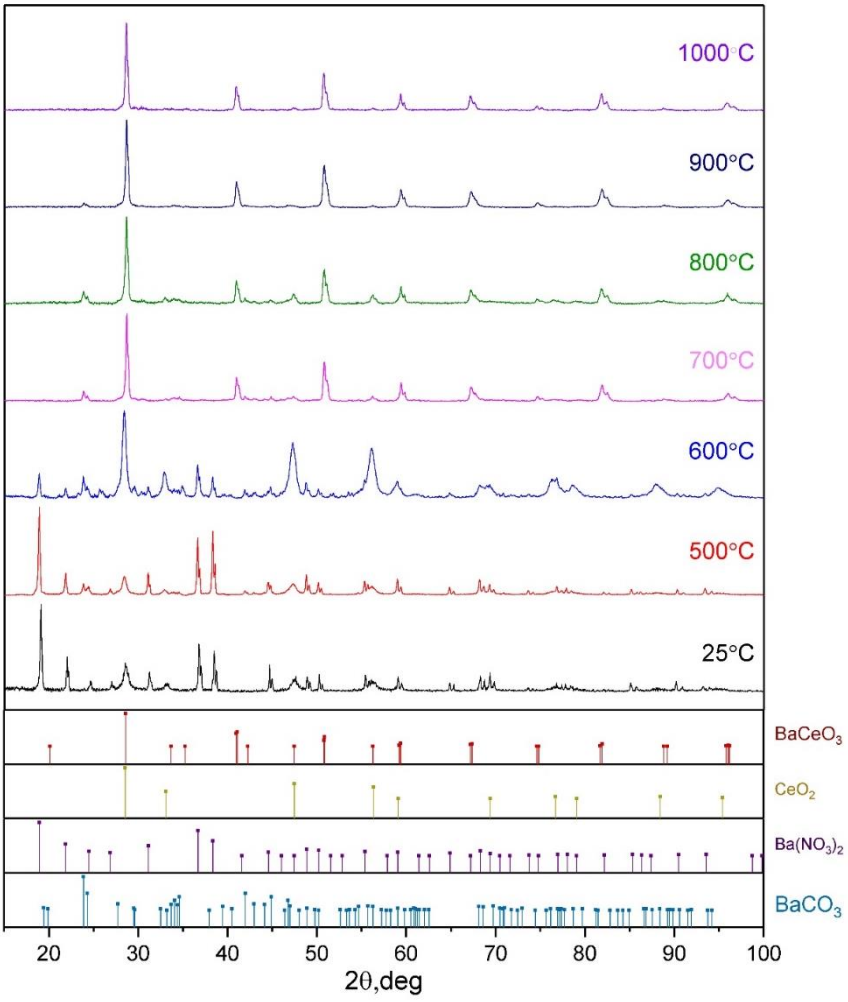

Fig. 3 XRD patterns of as-prepared and annealed $BaCeO_3$-based samples

The products of direct hydrazine-nitrate synthesis (as-prepared sample) contain phases of barium nitrate (cubic, P213, JCPDS#24-0053), cerium oxide (cubic, *Fm-3m*, JCPDS#34-0394) and barium carbonate (orthorhombic, *Pnma*, JCPDS#45-1471). During thermal processing at

temperatures of up to 500 °C no phase changes occur in the sample. As a consequence of thermal processing at 600 °C several changes were observed in the composition of the sample due to the decomposition of barium nitrate, which is in line with the results of thermal analysis (Fig. 2); also there occurs cerium oxide (IV) (crystallization of amorphous cerium oxide in the range of 500-600 °C) and the decomposition of barium carbonate $BaCO_3$ [14]. The composition of the sample processed thermally at 700 °C is in close correspondence with rhombic barium cerate, however, large amounts of barium carbonate and cerium oxide(IV) are also observed and their elimination occurs only at 1000 °C. Based on these results, the temperature of 1000 °C was chosen as the optimum temperature for obtaining chemically and phase-pure preceramic barium cerate powder as well as a sintered pellet based on it.

Table 1 – Phase evolution of powder after combustion synthesis

Phase/Temperature	*500*	*600*	*700*	*800*	*900*	*1000*
CeO_2	25	50	4	0	0	0
$BaCeO_3$	0	0	75	80	92	100
$BaCO_3$	-	25	21	20	8	0
$Ba(NO_3)_2$	75	26	0	0	0	0

Table 1 shows the results of quantitative analysis of a series of samples annealed in the temperature range of 500-1000 °C. The data is consistent with the results obtained by DTA-TGA.

Following the results of synchronic thermal and X-ray phase analyses, a scheme of physicochemical transformations was designed, as shown in Fig. 4.

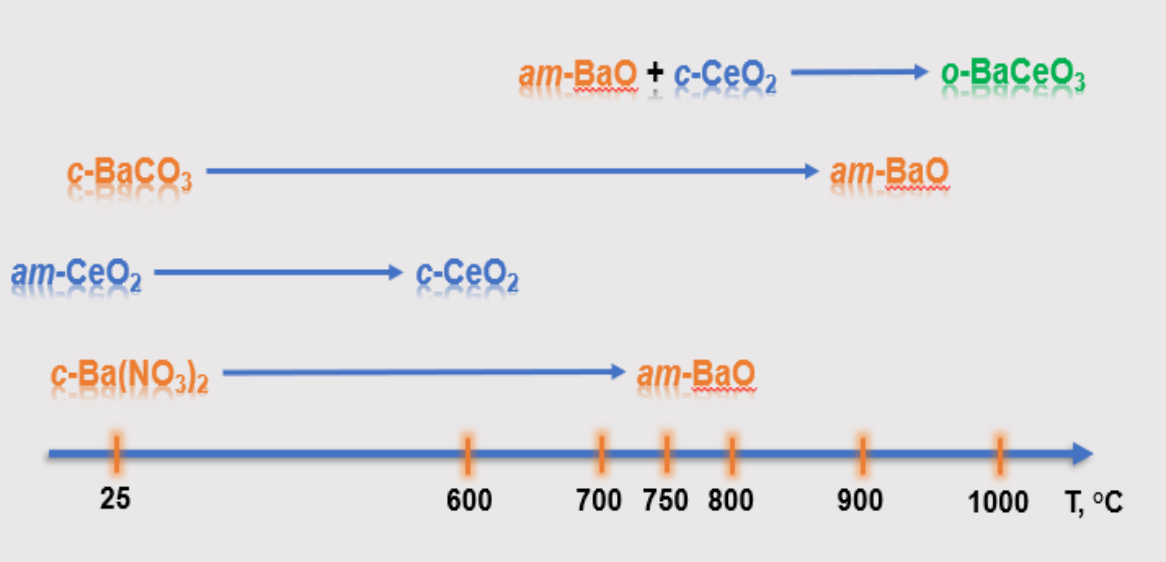

Fig. 4 Formation mechanism of $BaCeO_3$ preceramic powder via heat treatment of hydrazine-nitrate combustion products

3.2 Structural and morphological features of $BaCeO_3$

Refinement of the structure of barium cerate was performed using the Rietveld method. The results of the refinement, performed on the sample annealed at 1000 °C, are shown in Fig. 5. As can be concluded from the presented data, a considerable correspondence can be observed between experimental and theoretical diffractograms. The quality of the refinement process is characterized by the following values of R-factors: R_p = 8.03%, R_{wp} = 10.35%.

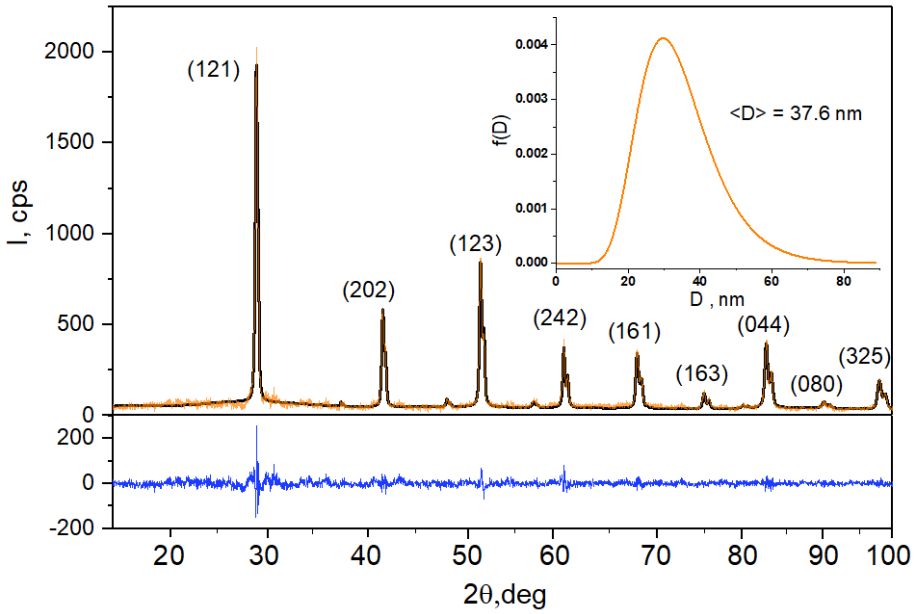

Fig. 5 Rietveld refinement results of $BaCeO_3$-based samples annealed at 1000 °C. Inset shows the crystallite size distribution of $BaCeO_3$

Based on the results of X-ray diffraction performed by the fundamental parameters method, the distribution of $BaCeO_3$ crystallites was measured. This data about the 1000 °C annealed sample is shown in the inset in Fig. 5. The crystallites have a narrow size distribution at the average size of (<D>) 37.6 nm and width of the distribution of (FWHM) 21.8 nm. The obtained size values of crystallites are noticeably lower than those of barium cerate synthesized by a solid-state method – 45-47 nm [34], 50 nm [19], or citrate methods – 240 nm [20], – 97 nm [35].

Table 2 shows the parameters of a unit cell and the average size of $BaCeO_3$ crystallites refined by the Rietveld method and annealed at the temperatures of 700, 800, 900 and 1000 °C from the products of hydrazine-nitrate combustion.

Table 2 Rietveld refinement results of $BaCeO_3$-based samples

Temperature Parameter	***700***	***800***	***900***	***1000***
a, Å	6.2129(19)	6.211(6)	6.2351(5)	6.2145(4)
b, Å	8.8016(9)	8.8060(12)	8.7741(7)	8.7776(6)
c, Å	6.209(2)	6.212(6)	6.2110(5)	6.2337(5)
V, Å³	339.53	339.76	339.79	340.04
α = β = γ, °	90	90	90	90

<D>, nm	35.4±2.0	33.4±2.0	36.9±2.0	37.6±2.0
R_{wp}, %	11.52	10.48	11.77	10.35
R_p, %	8.64	8.01	8.57	8.03

The refined parameters correspond to known crystallographic data of barium cerate with rhombic structure (*a*= 6.2517 Å, *b*= 8.7906 Å and *c*= 6.2271 Å, *V*=342.218 Å^3, *Pmna* space group) [36]. On the diffractogram of the $BaCeO_3$ annealed at 1000 °C reflexes of other phases were not detected. Increasing temperature causes unsystematic changes in the parameters of the unit cell - its size slightly increases with the rise of temperature, which is likely the result of the growing refinement of the crystallite structure of obtained barium cerate nanocrystals.

Morphological characteristics of the as-prepared samples annealed at 700 °C and 1000 °C were investigated through the scanning electron microscopy the results of which are presented in Fig. 6.

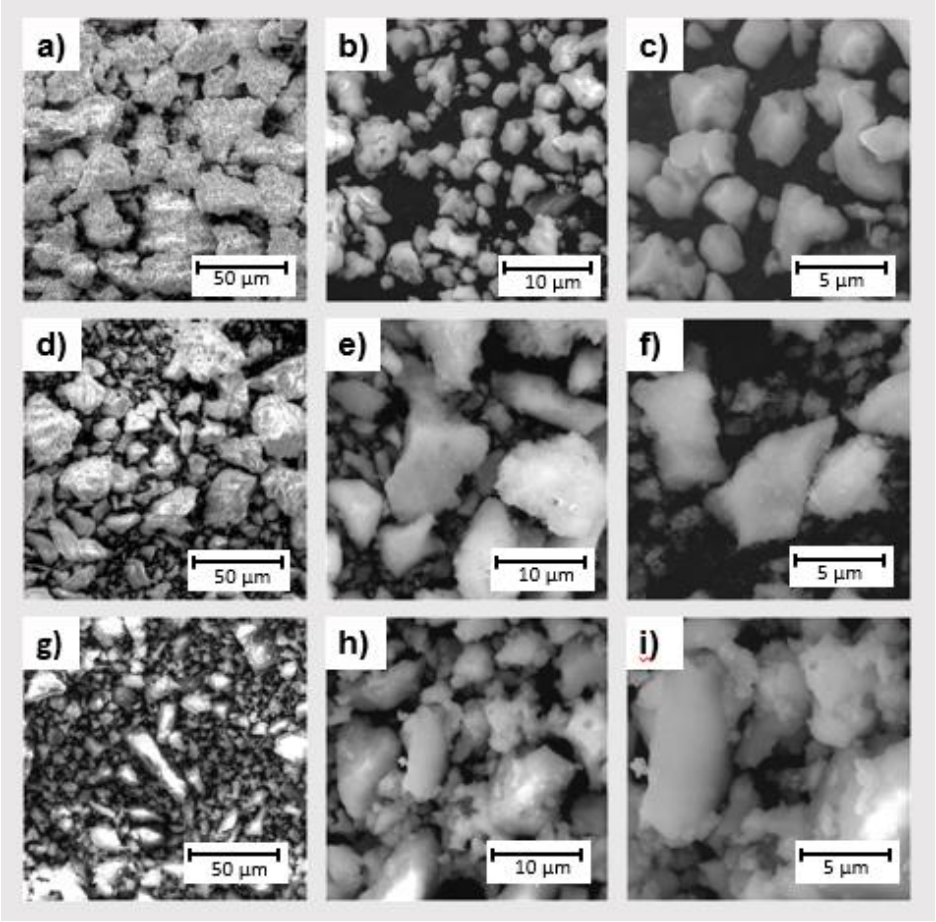

Fig. 6 SEM images of as-prepared (a-c) and annealed at 700 °C (d-f) and at 1000 °C (g-i) $BaCeO_3$-based samples

The above results indicate that the $BaCeO_3$-based sample annealed at 1000 °C was strongly agglomerated into micron- and submicron-sized structures.

The degree of agglomeration changes in as-prepared samples depending on the temperature of processing: with the rise of temperature a tendency for decreasing the size of agglomerates is observed, which is connected with the intense decomposition of intermediate products in the process of obtaining barium cerate. (Fig. 2,3).

In the original sample, the sizes of agglomerates vary in the range of 20 – 50 μm; in the sample annealed at 700 °C, the sizes of agglomerates do not exceed 40 μm. The sample annealed at 1000 °C, according to the XRD data, is represented by a single phase-orthorhombic barium cerate and is comprised predominantly of agglomerates not exceeding the size of 20 μm. All samples are characterized by the narrow size distribution of agglomerates.

The sample annealed at 1000 °C, following the data of quantitative and qualitative analysis, consists of barium cerate nanoparticles.

To analyze the specific surface and porosity structures of the annealed samples adsorption-structural analysis was performed. Fig. 7 shows adsorption isotherms of samples annealed at temperatures from 700 °C to 1000 °C, as well as the values of corresponding surface areas (see inset in Fig. 7).

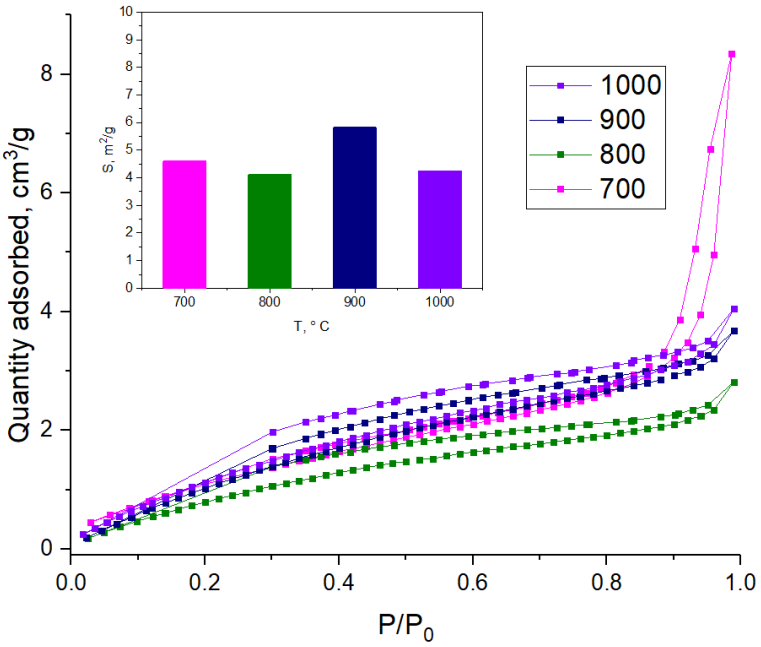

Fig. 7 N_2 adsorption-desorption isotherms of $BaCeO_3$-based samples annealed at 700, 800, 900 and 1000 °C. Inset shows corresponding specific surface areas

According to the IUPAC classification, the isotherms presented above belong to type II, and the observed hysteresis loops – to type H1. The porosity of the obtained powders varies from 11.2% in the sample synthesized at 700 °C to 4.7% in the sample synthesized at 1000 °C. The

values of specific surface structures range from 4.1 m^2/g to 5.8 m^2/g, depending on the temperature of annealing.

The values of specific surface structure are close to those obtained in other works: 4.46 m^2/g [20], 3.4 m^2/g [21], 3 m^2/g [22], 3 m^2/g [37]. However, some works [38] reported slightly higher values of specific surface structure - 6-8 m^2/g.

3.3 Thermophysical properties

Sample annealed at 1000 °C was selected as the basis for obtaining a sintered pellet due to its high chemical and phase uniformity. Sample formed from the annealed powders at a pressure of 25 bar and sintered at the final temperature (1000 ± 10°C) in an electric furnace in the air by heating to the final temperature at 20°C/min and holding there for 4 h. To estimate the potential of this sample as a preceramic powder, its density characteristics were analyzed at the formed pellet. The results of the analysis are shown in Table 3.

Table 3 Density characteristics of $BaCeO_3$-based sintered pellet

Parameter	*Value*
ρ_{XRD}, g/cm^3	6.36 (100%)
ρ_{pyc} g/cm^3	5.54 (87%)
ρ_{bulk} g/cm^3	3.80 (69%)
P_{open},%	12.90
P_{closed}, %	27.34
P_{total}, %	40.25

According to the data presented in work [16], the density of barium cerate in the case of solid-state synthesis does not exceed 70%, while obtaining it via the nitrate method results in a density of about 80% - conditional upon prolonged annealing. Finally, using the method of coprecipitation of oxalates with subsequent annealing results in values of 85-90%. In work [42] the density of barium cerate with various dopants is characterized by values of > 95%. Consequently, the nanocrystallite $BaCeO_3$ obtained in this work has density and porosity characteristics that correspond to known preceramic powders based on barium cerate, which lends to the conclusion that it can be used in this capacity.

Fig. 8 shows the results of measurements of thermal diffusivity and thermal conductivity of the pellet sintered at 1000 °C.

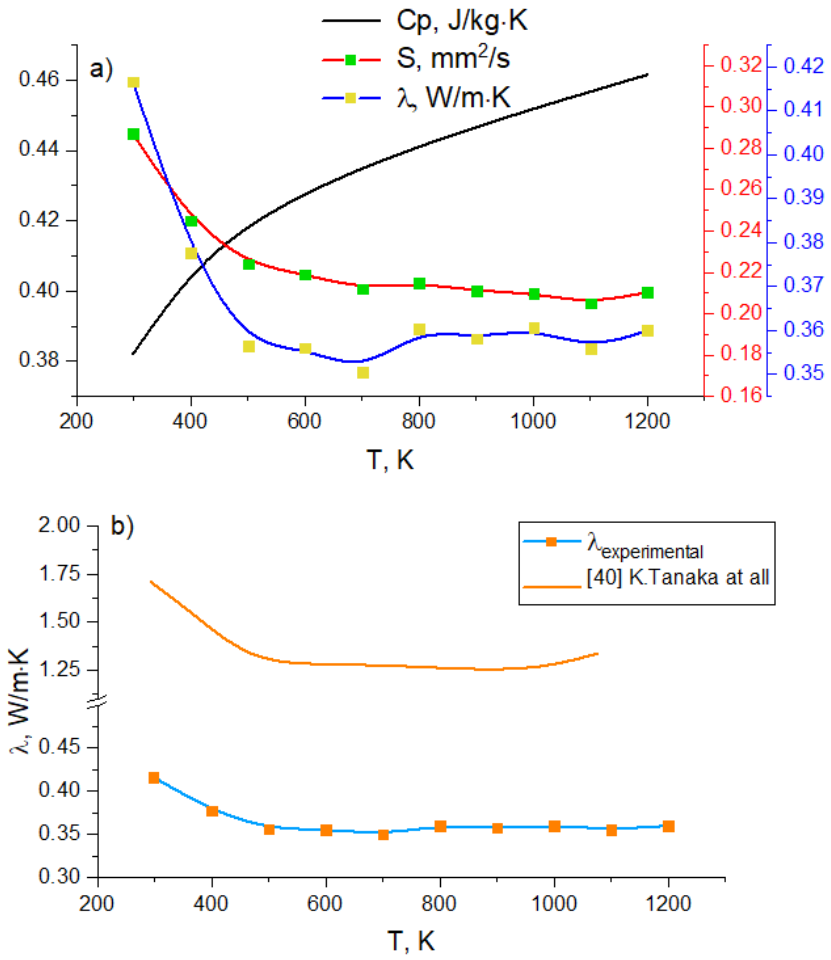

Fig. 8 Temperature dependence of thermal diffusivity, heat capacities and thermal conductivities of $BaCeO_3$ sintered at 1000 °C (a) and comparison of thermal conductivity dependencies of the sintered pellet (this work) and dense ceramics (work [40]) (b)

At room temperature, the value of thermal diffusivity is 0.28 mm^2/s, and with the rise of temperature, it decreases to 0.20 mm^2/s at 1100K. The thermal conductivity of the sintered material varies from 0.41 to 0.35 W/m·K in the same temperature interval. The temperature dependence of the thermal conductivities of $BaCeO_3$ shows typical phonon conduction characteristics [39], the thermal conductivities decrease with increasing temperature. Ba and Sr series perovskite compounds follow the general rule for predicting the magnitude of thermal conductivity, i.e., a material with high formula weight and with low Debye temperature exhibits low thermal conduction [40]. The data on the thermal conductivity of barium cerate in the work [40] varies from 1.33 to 1.70 W/m·K for nonporous material. The thermal conductivity values for the sintered pellet obtained in this work are noticeably lower than those for dense ceramics but the temperature dependence process is analogical. Considering that the porosity of the obtained pellet constitutes practically 40%, then in the case of obtaining dense ceramics from the $BaCeO_3$ preceramic powder

synthesized by hydrazine-nitrate combustion, the possibility of obtaining higher thermoconductive properties of ceramics is beyond any doubt.

4. Conclusions

In this work chemically and phase-pure preceramic powder of barium cerate was obtained using hydrazine-nitrate combustion. It was demonstrated that using hydrazine as fuel has the advantage of the lack of carbon residue in the combustion products, which significantly lowers the formation of carbonate impurities. It was concluded that hydrazine-nitrate combustion allows to obtain $BaCeO_3$ with crystallite sizes smaller than in the case of solid-state and nitrate synthesis – and with narrower size distribution. It was demonstrated that the thermophysical properties of the sintered sample based on the preceramic powder is analogical to the thermophysical properties of densely sintered ceramics based on $BaCeO_3$, which allows expecting successful application of this method in obtaining ceramic materials and products. Since the solution combustion method (including hydrazine-nitrate combustion) allows diverse and controlled doping of preceramic powders with d- and f-elements, further development of this method will provide the means to obtain new ceramic materials based on barium cerate for SOFC components and devices.

Acknowledgments

The studies were performed using the analytical equipment of the Engineering Center of the St. Petersburg State Institute of Technology. The authors are especially grateful to M.I. Chebanenko, K.D. Martinson, D.P. Danilovich. and Motaylo E.S. for help in characterizing the materials and D.K. Przybyla for help with translating the text of the article.

References

[1] B. Shri Prakash, R. Pavitra, S. Senthil Kumar, S.T. Aruna, Electrolyte bi-layering strategy to improve the performance of an intermediate temperature solid oxide fuel cell: A review, J. Power Sources. 381 (2018) 136–155. https://doi.org/10.1016/j.jpowsour.2018.02.003.

[2] F.S. da Silva, T.M. de Souza, Novel materials for solid oxide fuel cell technologies: A literature review, Int. J. Hydrogen Energy. 42 (2017) 26020–26036. https://doi.org/10.1016/j.ijhydene.2017.08.105.

[3] D. Panthi, N. Hedayat, Y. Du, Densification behavior of yttria-stabilized zirconia powders for solid oxide fuel cell electrolytes, J. Adv. Ceram. 7 (2018) 325–335. https://doi.org/10.1007/s40145-018-0282-4.

[4] C. Liu, H. Zhang, J. Xia, Z. Li, Synthesis and characterization of $Zr_{0.85}Y_{0.15}O_{1.925}$-$La_{9.33}Si_6O_{26}$ composite electrolyte for application in SOFCs, J. Adv. Ceram. 1 (2012) 327–335. https://doi.org/10.1007/s40145-012-0033-x.

[5] A. Jun, J. Kim, J. Shin, G. Kim, Perovskite as a Cathode Material: A Review of its Role in Solid-Oxide Fuel Cell Technology, ChemElectroChem. 3 (2016) 511–530. https://doi.org/10.1002/celc.201500382.

[6] L. Shu, J. Sunarso, S.S. Hashim, J. Mao, W. Zhou, F. Liang, Advanced perovskite anodes for solid oxide fuel cells: A review, Int. J. Hydrogen Energy. 44 (2019) 31275–31304. https://doi.org/10.1016/j.ijhydene.2019.09.220.

[7] S. Afroze, A.H. Karim, Q. Cheok, S. Eriksson, A.K. Azad, Latest development of double perovskite electrode materials for solid oxide fuel cells: a review, Front. Energy. 13 (2019) 770–797. https://doi.org/10.1007/s11708-019-0651-x.

[8] J. Sunarso, S.S. Hashim, N. Zhu, W. Zhou, Perovskite oxides applications in high temperature oxygen separation, solid oxide fuel cell and membrane reactor: A review, Prog. Energy Combust. Sci. 61 (2017) 57–77. https://doi.org/10.1016/j.pecs.2017.03.003.

[9] D. Medvedev, A. Murashkina, E. Pikalova, A. Demin, A. Podias, P. Tsiakaras, $BaCeO_3$: Materials development, properties and application, Prog. Mater. Sci. 60 (2014) 72–129. https://doi.org/10.1016/j.pmatsci.2013.08.001.

[10] K. Xie, R. Yan, X. Chen, D. Dong, S. Wang, X. Liu, G. Meng, A new stable $BaCeO_3$-based proton conductor for intermediate-temperature solid oxide fuel cells, J. Alloys Compd. 472 (2009) 551–555. https://doi.org/10.1016/j.jallcom.2008.05.036.

[11] J. Lyagaeva, N. Danilov, G. Vdovin, J. Bu, D. Medvedev, A. Demin, P. Tsiakaras, A new Dy-doped $BaCeO_3$-$BaZrO_3$ proton-conducting material as a promising electrolyte for reversible solid oxide fuel cells, J. Mater. Chem. A. 4 (2016) 15390–15399. https://doi.org/10.1039/c6ta06414k.

[12] D.A. Medvedev, A.A. Murashkina, A.K. Demin, Formation of dense electrolytes based on $BaCeO_3$ and $BaZrO_3$ for application in solid oxide fuel cells: The role of solid-state reactive sintering, Rev. J. Chem. 5 (2015) 193–214. https://doi.org/10.1134/s2079978015030024.

[13] M. Zolkos, The Democratic Impact of International Organizations, Int. Stud. Rev. 7 (2005) 478–480. https://doi.org/10.1111/j.1551-2916.2005.00521.x.

[14] R. Verbov, V. Kavecansk, P. Diko, V. Antal, Synthesis of nanocrystalline $BaCeO_3$ by oxalate coprecipitation for $YBa_2Cu_3O_7$ bulk superconductors, Acta Phys. Pol. A. 133 (2018) 82–85. https://doi.org/10.12693/APhysPolA.133.82.

[15] D.W. Lee, J.H. Won, K.B. Shim, Low temperature synthesis of $BaCeO_3$ nano powders by the citrate process, Mater. Lett. 57 (2003) 3346–3351. https://doi.org/10.1016/S0167-577X(03)00072-7.

[16] G.N. Glavee, R.D. Hunt, M. Paranthaman, Low temperature preparation of $BaCeO_3$ and $Ce_{0.75}Zr_{0.25}O_2$ thin films using sol-gel processing techniques, Mater. Res. Bull. 34 (1999) 817–825. https://doi.org/10.1016/S0025-5408(99)00061-6.

[17] K. Ouzaouit, A. Benlhachemi, H. Benyaich, J.P. Dallas, S. Villain, J.A. Musso, J.R. Gavarri, Electrical conductivity of $BaCeO_3$ synthesized by new sol-gel method Lattice Pnma Pnma, Powder Diffr. 7 (2006) 94–97.

[18] A. V. Orlov, O.A. Shlyakhtin, A.L. Vinokurov, A. V. Knotko, Y.D. Tret'yakov, Preparation and properties of fine $BaCeO_3$ powders for low-temperature sintering, Inorg. Mater. 41 (2005) 1194–1200. https://doi.org/10.1007/s10789-005-0286-7.

[19] D. Medvedev, V. Maragou, E. Pikalova, A. Demin, P. Tsiakaras, Novel composite solid state electrolytes on the base of $BaCeO_3$ and CeO_2 for intermediate temperature electrochemical devices, J. Power Sources. 221 (2013) 217–227. https://doi.org/10.1016/j.jpowsour.2012.07.120.

[20] F.W. Bezerra Lopes, M. Arab, H.P. Macedo, C.P. de Souza, J.F. de Souza, J.R. Gavarri, High temperature conduction and methane conversion capability of $BaCeO_3$ perovskite, Powder Technol. 219 (2012) 186–192. https://doi.org/10.1016/j.powtec.2011.12.039.

[21] J. Wang, C. Huang, X. Chen, H. Zhang, Z. Li, Z. Zou, Photocatalytic CO_2 reduction of $BaCeO_3$ with 4f configuration electrons, Appl. Surf. Sci. 358 (2015) 463–467. https://doi.org/10.1016/j.apsusc.2015.08.063.

[22] E. Kalinina, E. Pikalova, A. Kolchugin, N. Pikalova, A. Farlenkov, Comparative study of electrophoretic deposition of doped $BaCeO_3$-based films on $La_2NiO_{4+\delta}$ and $La_{1.7}Ba_{0.3}NiO_{4+\delta}$ cathode substrates, Materials (Basel). 12 (2019). https://doi.org/10.3390/ma12162545.

[23] V.I. Popkov, O. V. Almjasheva, V. V. Panchuk, V.G. Semenov, V. V. Gusarov, The role of pre-nucleus states in formation of nanocrystalline yttrium orthoferrite, Dokl. Chem. 471 (2016) 356–359. https://doi.org/10.1134/S0012500816120041.

[24] V.I. Popkov, O. V. Almjasheva, V. V. Gusarov, The investigation of the structure control possibility of nanocrystalline yttrium orthoferrite in its synthesis from amorphous powders, Russ. J. Appl. Chem. 87 (2014) 1417–1421. https://doi.org/10.1134/S1070427214100048.

[25] V.I. Popkov, O. V. Almjasheva, M.P. Schmidt, S.G. Izotova, V. V. Gusarov, Features of nanosized $YFeO_3$ formation under heat treatment of glycine-nitrate combustion products, Russ. J. Inorg. Chem. 60 (2015) 1193–1198. https://doi.org/10.1134/S0036023615100162.

[26] G. Liu, J. Li, K. Chen, Combustion synthesis of refractory and hard materials: A review, Int. J. Refract. Met. Hard Mater. 39 (2013) 90–102. https://doi.org/10.1016/j.ijrmhm.2012.09.002.

[27] A. Varma, A.S. Mukasyan, A.S. Rogachev, K. V. Manukyan, Solution Combustion Synthesis of Nanoscale Materials, Chem. Rev. 116 (2016) 14493–14586. https://doi.org/10.1021/acs.chemrev.6b00279.

[28] K.C. Patil, S.T. Aruna, T. Mimani, Combustion synthesis: An update, Curr. Opin. Solid State Mater. Sci. 6 (2002) 507–512. https://doi.org/10.1016/S1359-0286(02)00123-7.

[29] K.D. Martinson, I.S. Kondrashkova, V.I. Popkov, Synthesis of $EuFeO_3$ nanocrystals by glycine-nitrate combustion method, Russ. J. Appl. Chem. 90 (2017) 1214–1218. https://doi.org/10.1134/S1070427217080031.

[30] I.S. Kondrashkova, K.D. Martinson, N. V. Zakharova, V.I. Popkov, Synthesis of Nanocrystalline $HoFeO_3$ Photocatalyst via Heat Treatment of Products of Glycine-Nitrate Combustion, Russ. J. Gen. Chem. 88 (2018) 2465–2471. https://doi.org/10.1134/S1070363218120022.

[31] V.I. Popkov, V.P. Tolstoy, V.G. Semenov, Synthesis of phase-pure superparamagnetic nanoparticles of $ZnFe_2O_4$ via thermal decomposition of zinc-iron layered double hydroxysulphate, J. Alloys Compd. 813 (2020) 152179. https://doi.org/10.1016/j.jallcom.2019.152179.

[32] V.I. Popkov, O. V. Almjasheva, V.N. Nevedomskiy, V. V. Panchuk, V.G. Semenov, V. V. Gusarov, Effect of spatial constraints on the phase evolution of $YFeO_3$-based nanopowders under heat treatment of glycine-nitrate combustion products, Ceram. Int. 44 (2018) 20906–20912. https://doi.org/10.1016/j.ceramint.2018.08.097.

[33] V.V. Zvereva, V.I. Popkov, Synthesis of CeO_2 -Fe_2O_3 nanocomposites via controllable oxidation of $CeFeO_3$ nanocrystals, Ceram. Int. 45 (2019) 12516–12520. https://doi.org/10.1016/j.ceramint.2019.03.188.

[34] J.H. Kim, Y.M. Kang, M.S. Byun, K.T. Hwang, Study on the chemical stability of Y-doped $BaCeO_{3-\delta}$ and $BaZrO_{3-\delta}$ films deposited by aerosol deposition, Thin Solid Films. 520 (2011) 1015–1021. https://doi.org/10.1016/j.tsf.2011.08.013.

[35] X.L. Yang, W.Q. Zhang, C.G. Xia, X.M. Xiong, X.Y. Mu, B. Hu, Low temperature ruthenium catalyst for ammonia synthesis supported on $BaCeO_3$ nanocrystals, Catal. Commun. 11 (2010) 867–870. https://doi.org/10.1016/j.catcom.2010.03.008.

[36] F. Genet, S. Loridant, C. Ritter, G. Lucazeau, Phase transitions in $BaCeO_3$: Neutron diffraction and Raman studies, J. Phys. Chem. Solids. 60 (1999) 2009–2021. https://doi.org/10.1016/S0022-3697(99)00031-1.

[37] E.G. Kalinina, E.Y. Pikalova, A.S. Farlenkov, Electrophoretic Deposition of Thin-Film Coatings of Solid Electrolyte Based on Microsize BaCeO3 Powders, Russ. J. Appl. Chem. 91 (2018) 934–941. https://doi.org/10.1134/S1070427218060095.

[38] A. Bassano, V. Buscaglia, M. Viviani, M. Bassoli, M.T. Buscaglia, M. Sennour, A. Thorel, P. Nanni, Synthesis of Y-doped $BaCeO_3$ nanopowders by a modified solid-state process and conductivity of dense fine-grained ceramics, Solid State Ionics. 180 (2009) 168–174. https://doi.org/10.1016/j.ssi.2008.12.026.

[39] S. Yamanaka, T. Hamaguchi, T. Oyama, T. Matsuda, S. ichi Kobayashi, K. Kurosaki, Heat capacities and thermal conductivities of perovskite type $BaZrO_3$ and $BaCeO_3$, J. Alloys Compd. 359 (2003) 1–4. https://doi.org/10.1016/S0925-8388(03)00137-3.

[40] K. Tanaka, I. Sato, T. Hirosawa, K. Kurosaki, H. Muta, S. Yamanaka, Thermophysical properties of perovskite type alkaline-earth metals and plutonium complex oxides, J. Nucl. Mater. 422 (2012) 163–166. https://doi.org/10.1016/j.jnucmat.2011.12.036.

Figures

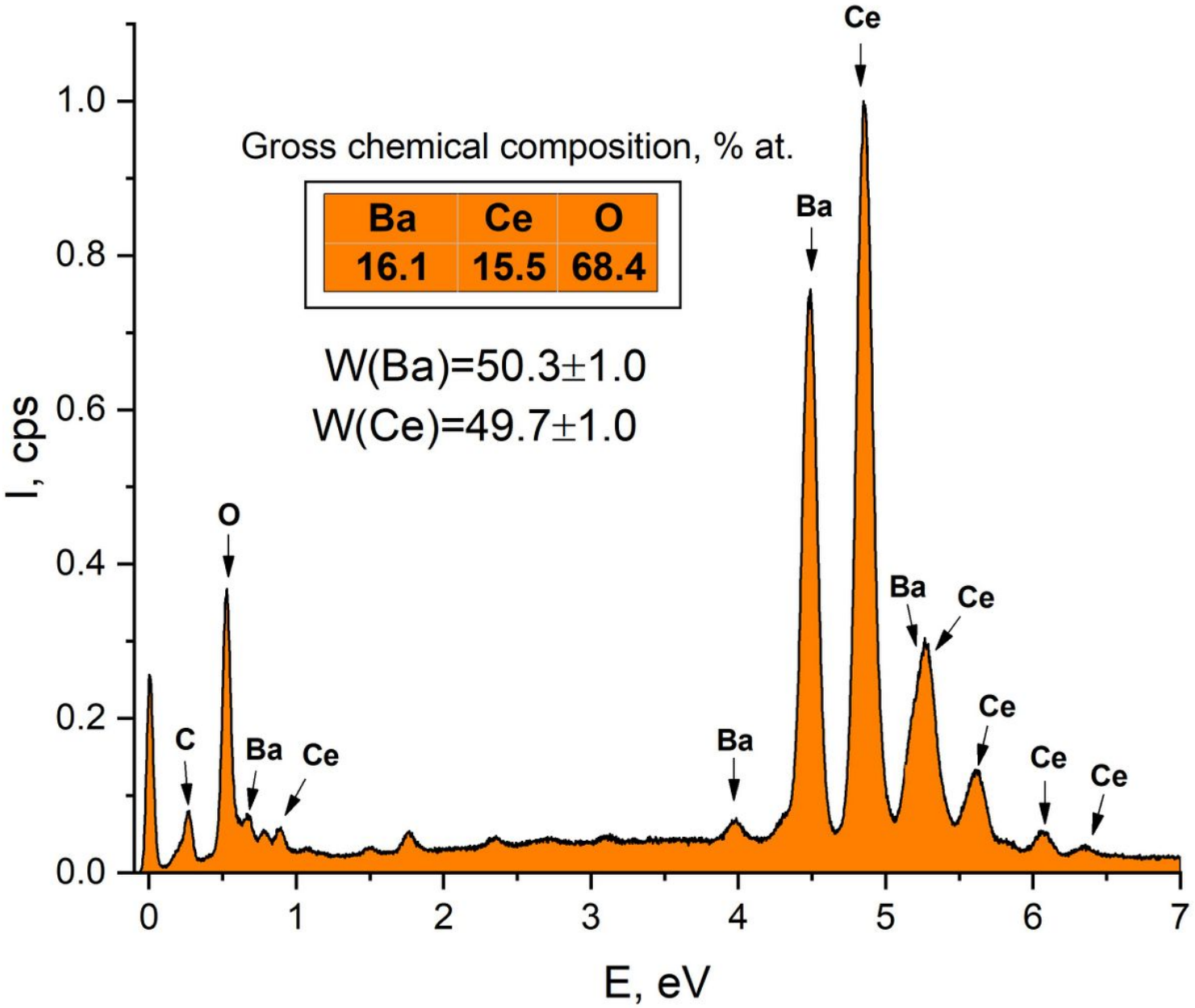

Figure 1

Energy dispersive spectrum of BaCeO3-based sample annealed at 1000 °C

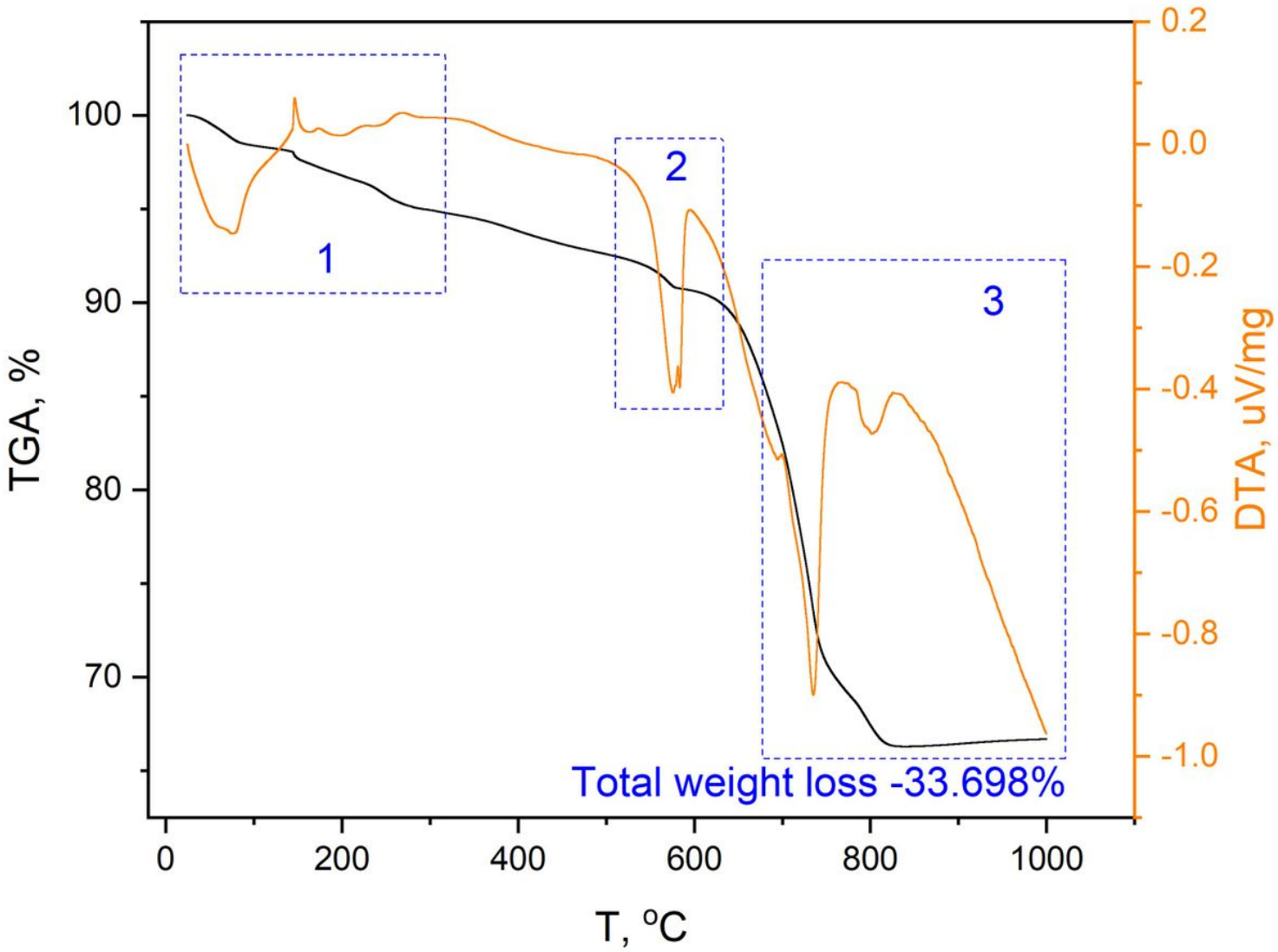

Figure 2

TGA-DTA thermograms of the as-prepared sample

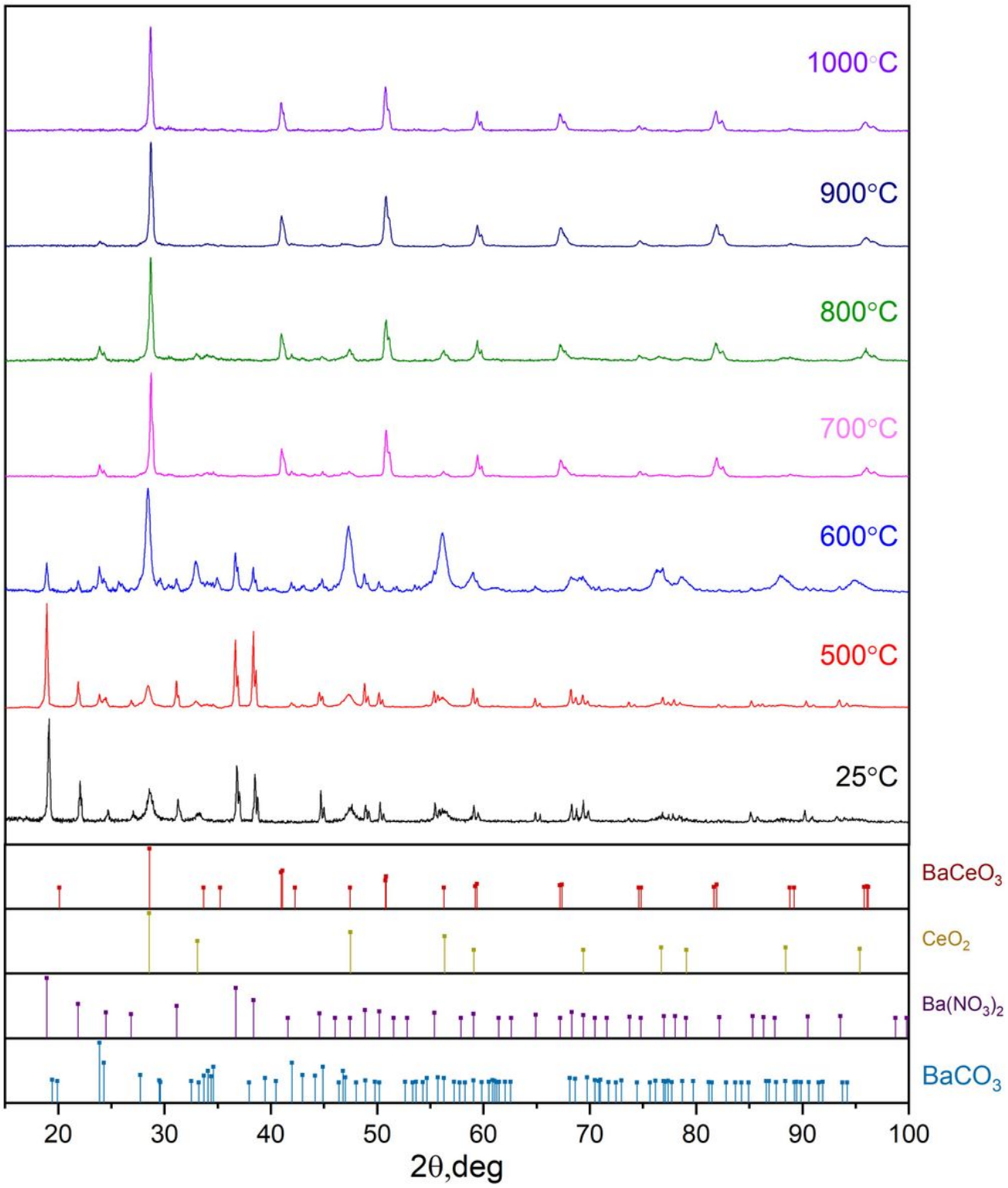

Figure 3

XRD patterns of as-prepared and annealed BaCeO3-based samples

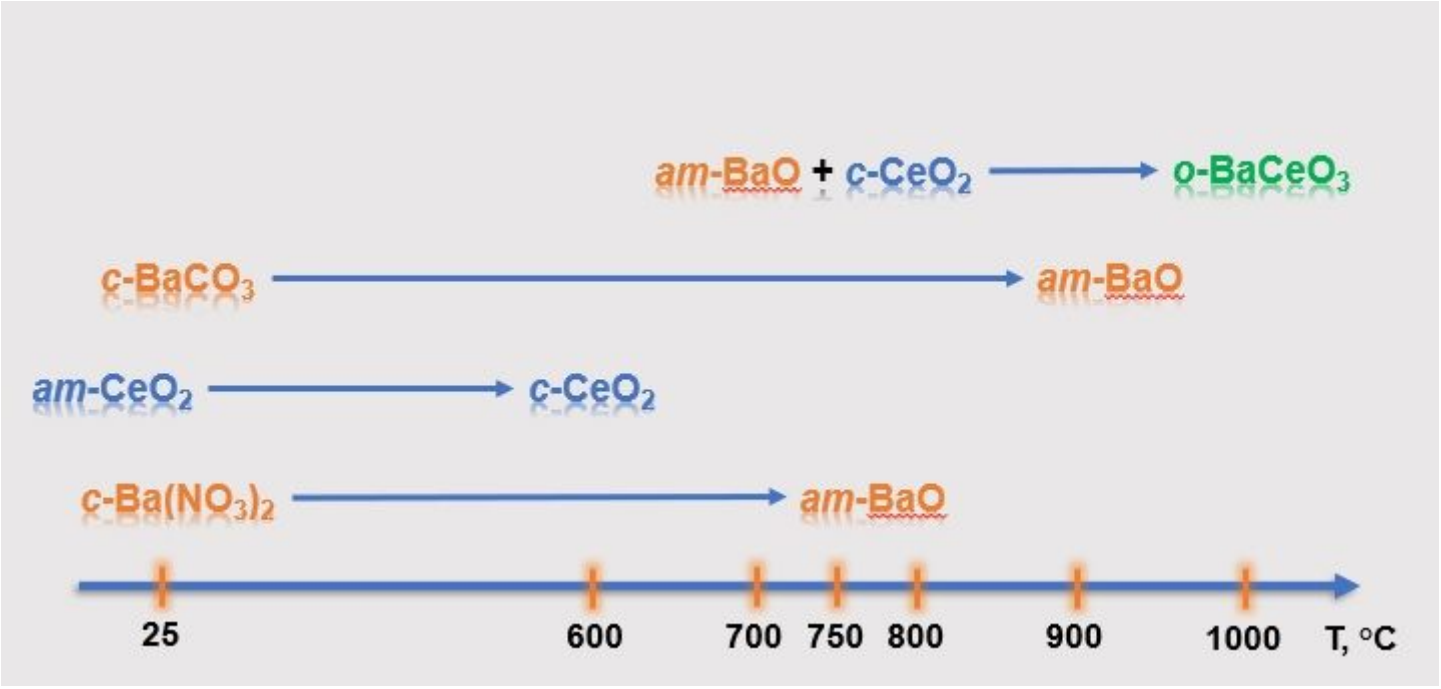

Figure 4

Formation mechanism of BaCeO3 preceramic powder via heat treatment of hydrazine-nitrate combustion products

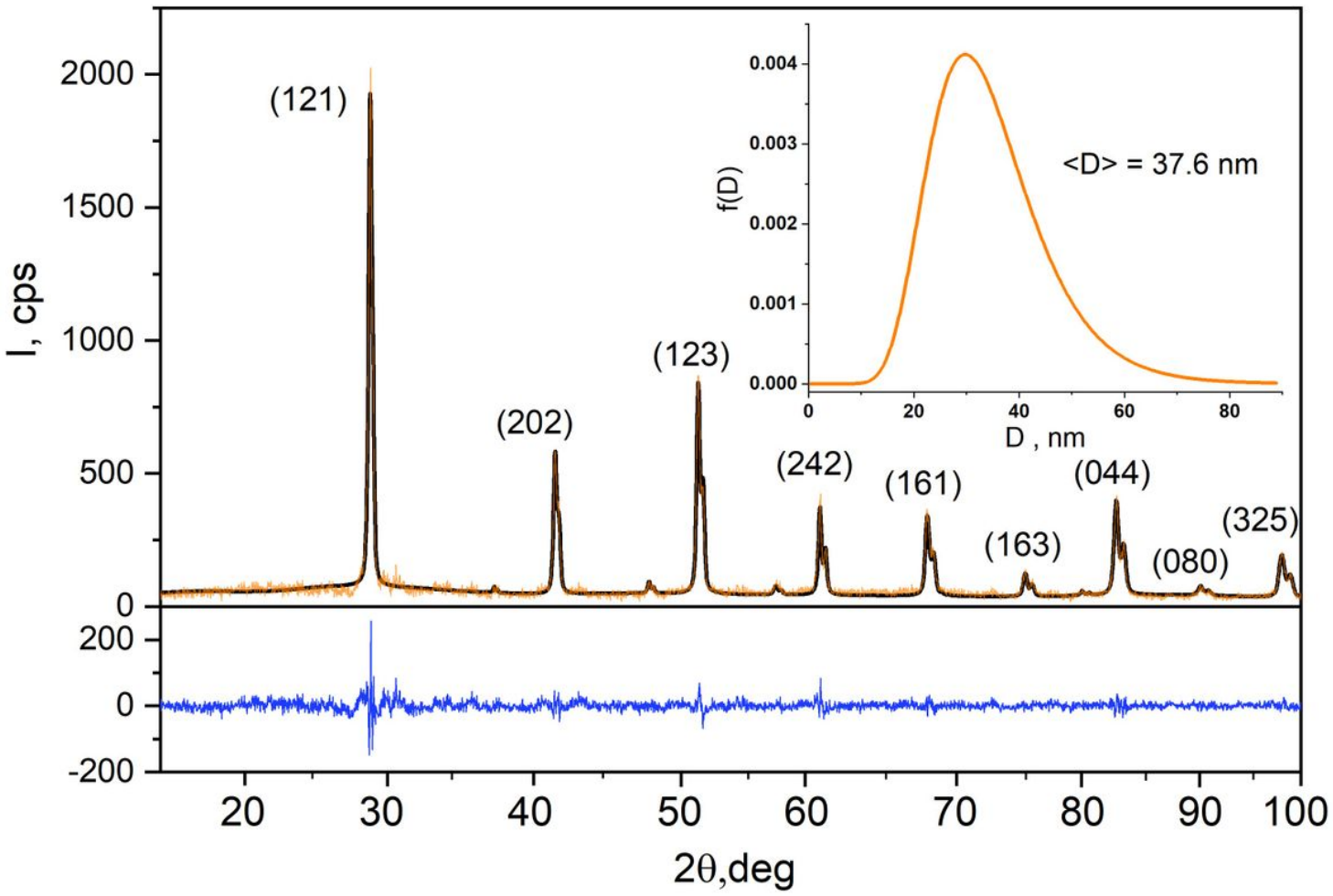

Figure 5

Rietveld refinement results of BaCeO¬3-based samples annealed at 1000 °C. Inset shows the crystallite size distribution of BaCeO3

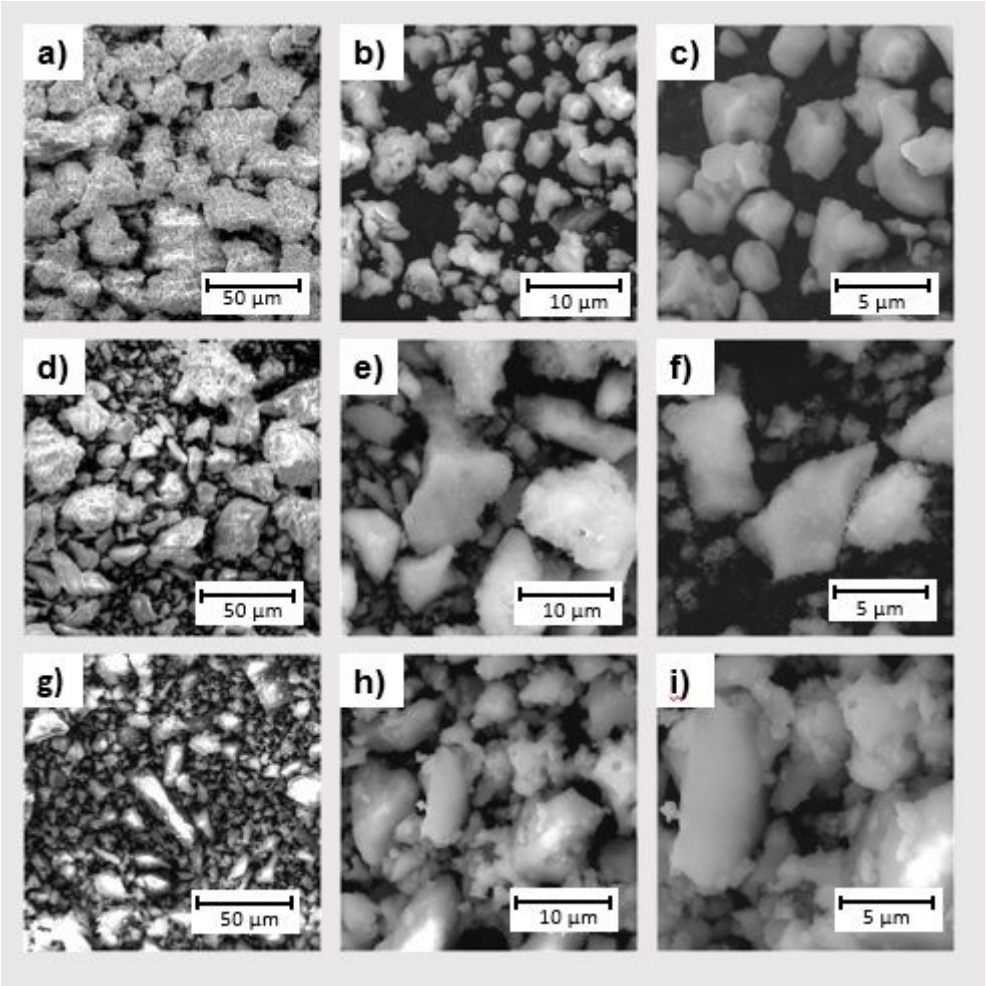

Figure 6

SEM images of as-prepared (a-c) and annealed at 700 °C (d-f) and at 1000 °C (g-i) BaCeO3-based samples

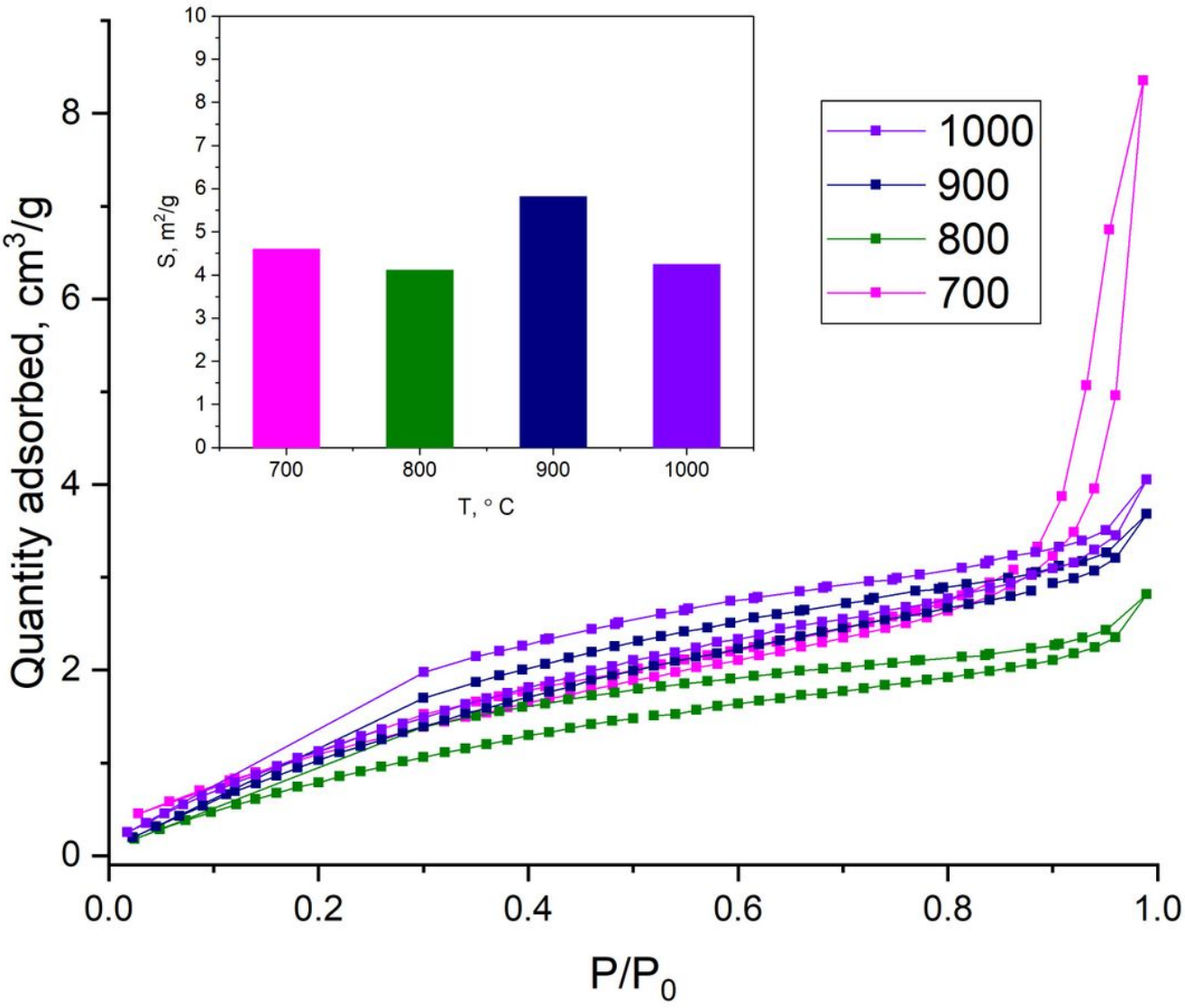

Figure 7

N2 adsorption-desorption isotherms of BaCeO3-based samples annealed at 700, 800, 900 and 1000 °C. Inset shows corresponding specific surface areas

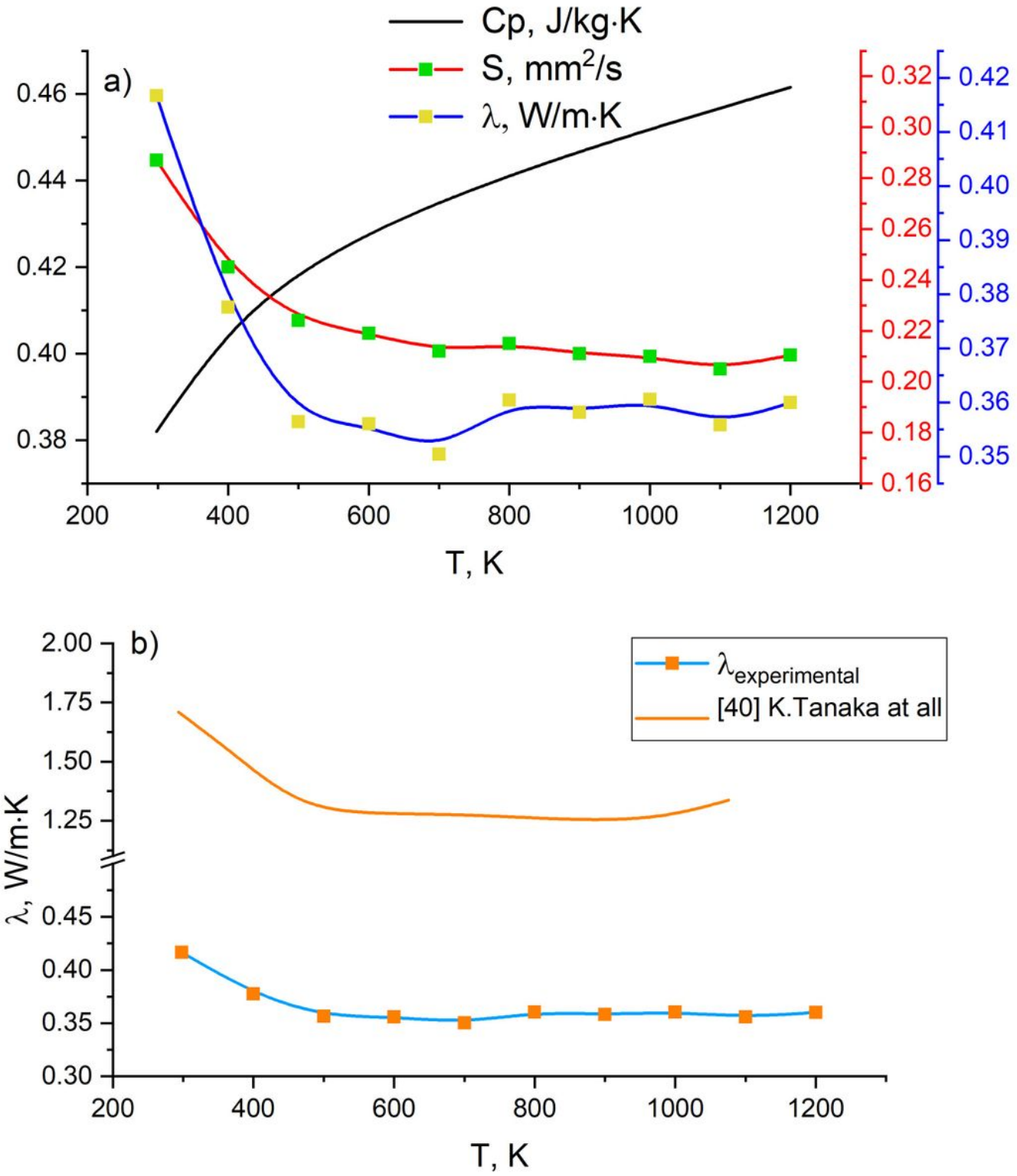

Figure 8

Temperature dependence of thermal diffusivity, heat capacities and thermal conductivities of BaCeO3 sintered at 1000 °C (a) and comparison of thermal conductivity dependencies of the sintered pellet (this work) and dense ceramics (work [40]) (b)